AGU PUBLICATIONS

Geophysical Research Letters

RESEARCH LETTER
10.1002/2015GL066473

Key Points:
- We relocate the 2015 Gorkha earthquakes using teleseismic and regional waveforms
- The main shock is located on the horizontal Main Himalaya Thrust (MHT) at a depth of 18.5 km
- Aftershocks show faulting structure in the hanging wall above the MHT

Supporting Information:
- Figures S1–S3 and Tables S1 and S2
- Bibliography S1

Correspondence to:
L. Bai,
bailing@itpcas.ac.cn

Citation:
Bai, L., H. Liu, J. Ritsema, J. Mori, T. Zhang, Y. Ishikawa, and G. Li (2016), Faulting structure above the Main Himalayan Thrust as shown by relocated aftershocks of the 2015 M_w7.8 Gorkha, Nepal, earthquake, *Geophys. Res. Lett.*, *43*, 637–642, doi:10.1002/2015GL066473.

Received 7 OCT 2015
Accepted 23 DEC 2015
Accepted article online 30 DEC 2015
Published online 23 JAN 2016

Faulting structure above the Main Himalayan Thrust as shown by relocated aftershocks of the 2015 M_w7.8 Gorkha, Nepal, earthquake

Ling Bai[1], Hongbing Liu[1], Jeroen Ritsema[2], James Mori[3], Tianzhong Zhang[4], Yuzo Ishikawa[5], and Guohui Li[1]

[1]Key Laboratory of Continental Collision and Plateau Uplift, Institute of Tibetan Plateau Research, Chinese Academy of Sciences, Beijing, China, [2]Department of Earth and Environmental Sciences, University of Michigan, Ann Arbor, Michigan, USA, [3]Disaster Prevention Research Institute, Kyoto University, Kyoto, Japan, [4]Institute of Geophysics, China Earthquake Administration, Beijing, China, [5]National Institute of Advanced Industrial Science and Technology, Tsukuba, Japan

Abstract The 25 April 2015, M_w7.8 Gorkha, Nepal, earthquake ruptured a shallow section of the Indian-Eurasian plate boundary by reverse faulting with NNE-SSW compression, consistent with the direction of current Indian-Eurasian continental collision. The Gorkha main shock and aftershocks were recorded by permanent global and regional arrays and by a temporary local broadband array near the China-Nepal border deployed prior to the Gorkha main shock. We relocate 272 earthquakes with $M_w > 3.5$ by applying a multiscale double-difference earthquake relocation technique to arrival times of direct and depth phases recorded globally and locally. We determine a well-constrained depth of 18.5 km for the main shock hypocenter which places it on the Main Himalayan Thrust (MHT). Many of the aftershocks at shallower depths illuminate faulting structure in the hanging wall with dip angles that are steeper than the MHT. This system of thrust faults of the Lesser Himalaya may accommodate most of the elastic strain of the Himalayan orogeny.

1. Introduction

The collision between the Indian and Eurasian continental plates formed the Himalaya mountain range, the highest orogenic belt on Earth with widespread continental seismicity. The region is classically divided into four tectonic units from south to north: Sub-Himalaya, Lesser Himalaya, Higher Himalaya, and Tethyan Himalaya [*Yin*, 2006] (Figure 1). The Main Frontal Thrust (MFT), Main Boundary Thrust (MBT), Main Central Thrust (MCT), and South Tibet Detachment (STD) separate the four tectonic units. They converge at the Main Himalaya Thrust (MHT), the detachment along which the Indian plate subducts beneath the Himalayan Mountains [*Ni and Barazangi*, 1984; *Zhao et al.*, 1993; *Nábělek et al.*, 2009].

The potential for devastating earthquakes in the Himalaya has long been recognized. Historical documents since the tenth century show evidence for great Himalayan earthquakes with a recurrence interval of about 800 years [*Kumar et al.*, 2010; *Bollinger et al.*, 2014]. Nearly 500 earthquakes of $M_w \geq 4.5$ have occurred along the Himalayas orogen since 1964. The Gorkha, Nepal, earthquake has heightened concern for large earthquakes along the Himalayan front [*Bilham*, 2015; *Hand and Pulla*, 2015]. This is the first well-recorded earthquake and aftershock sequence on a shallow portion of the MHT. The seismic data will provide new constraints on the fault zone structure of the Indian-Eurasian plate boundary at shallow depth and insight into seismic hazard in the region.

In this study, we relocate aftershock hypocenters to infer the structure of the Gorkha earthquake fault zone. Our data come from the Global Seismic Network, the China National Seismic Network, and a temporary array of 15 broadband seismic stations that we deployed at the China-Nepal border in December 2014. The combination of teleseimic (30–90°) *P* waveforms and regional *Pg*, *Sg*, *Pn*, and *Sn* signals is optimal for precise hypocenter determinations.

2. The Main Himalayan Thrust

The MHT is defined as the detachment that separates the underthrusting Indian plate from the overriding Himalaya orogeny. The concept of the MHT was proposed by *Ni and Barazangi* [1984] based on the locations

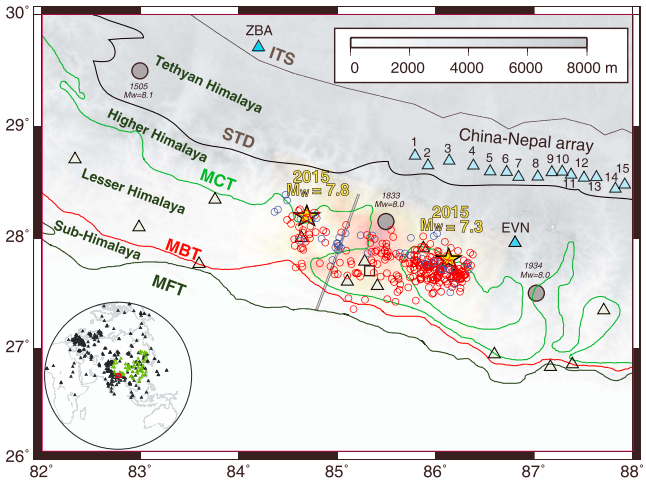

Figure 1. The study region showing the relocations of the M_w7.8 Gorkha, M_w7.3 Kodari earthquakes (yellow stars), aftershocks (red circles), and earthquakes that occurred before the Gorkha earthquake since 1980 (blue circles), which are superposed on a slip model [*Wang et al.*, 2015]. Historic seismicity of $M_w > 7.0$ since 1000 is shown with large black circles. Blue triangles show the 15 stations of the China-Nepal seismograph array deployed before the Gorkha earthquake. Green triangles show the short period seismic stations of the National Seismic Network of Nepal. Stations EVN and ZBA belong to the IO and CEDC networks, respectively. The square shows the location of Nepal's capital city, Kathmandu. The double lines indicate the location and the direction N20°E of the cross section shown in Figure 4. The inset at the lower left corner shows seismic stations from the China National Seismic Network (green triangles) and the Global Seismic Network (black triangles) used in this study.

and fault plane solutions of moderate earthquakes at 10–20 km depths. A similar concept of a Main Detachment Fault was put forward by *Schelling and Arita* [1991] from a tectonic reconstruction of eastern Nepal. The MHT was imaged at a depth of 30–40 km by *Zhao et al.* [1993] with a deep seismic reflection profile in southeastern Tibet. In the past decade, broadband seismic arrays have been deployed to constrain the structure of the MHT in the central [*Hetényi et al.*, 2007; *Nábělek et al.*, 2009; *Xu et al.*, 2015], eastern [*Schulte-Pelkum et al.*, 2005; *Acton et al.*, 2011], and western [*Rai et al.*, 2006; *Caldwell et al.*, 2013] Himalaya, respectively.

Subduction of the Indian continental lithosphere beneath the Himalaya has been shallow and nearly horizontal since the initiation of the Indo-Asian collision. The dip angle increases with depth from the MCT to the Indus-Tsangpo suture (ITS). The deeper sections of the MHT are constrained best [e.g., *Zhao et al.*, 1993]. However, the shallow structure of the MHT remains uncertain because the interpretation of shallow seismic wave refraction is difficult [*Hetényi et al.*, 2007; *Nábělek et al.*, 2009].

3. Waveform Modeling and Multiscale Double-Difference Earthquake Relocations

We relocate a total of 272 earthquakes, including the Gorkha main shock, 233 aftershocks within 1 month and 38 earthquakes that occurred before the Gorkha earthquake since 1980 (Figure 1 and Table S2 in the supporting information). Our estimates are based on five data sets: (1) bulletins from the National Earthquake Information Center (NEIC) of the U.S. Geological Survey for 234 earthquakes of $M_w > 3.5$ that occurred within 1 month after the main shock, (2) bulletins from the National Seismic Network of Nepal and the International Seismological Centre (ISC) for 38 earthquakes of $M_w > 3.5$ that occurred in the source region during three decades prior to the Gorkha earthquake, (3) seismic and waveform data from the China Earthquake Data Center (CEDC) and the China National Seismic Network (CNSN), (4) teleseismic *P* waveforms from the Global Seismic Network, and (5) waveform data from a temporary array of 15 broadband seismic stations along the China-Nepal border, deployed by the Institute of Tibetan Plateau Research, Chinese Academy of Sciences, prior to the Gorkha earthquake. Our local temporary array recorded many of the aftershocks at epicentral distances less than 100 km (Figure 2a), including the $M_w > 7.3$ Kodari earthquake [*Lindsey et al.*, 2015]. Permanent seismic stations in the Tibetan region at epicentral distances of 2–7° recorded clear *Pn* and *Sn* head waves and *Pg* and *Sg* waves (Figure 2b). At teleseismic distances, surface reflections *pP* and *sP* phases for moderate earthquakes (Figure 3) provide constraints on focal depths.

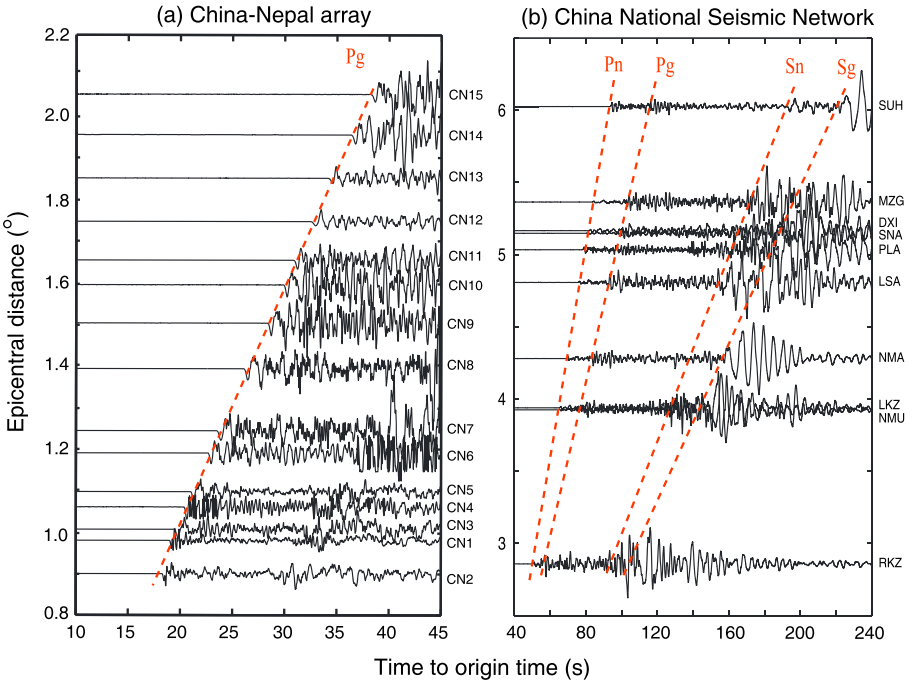

Figure 2. Record section of vertical-component seismograms for event 222 (Table S2) recorded by the (a) China-Nepal array and (b) China National Seismic Network. Dotted red lines are observed arrival times of each phase.

Our analysis comprises three steps. First, we determine hypocenters for the Gorkha earthquake and its 233 aftershocks based on the HYPOSAT methodology [*Schweitzer*, 2001]. Absolute traveltimes and traveltime differences at common stations are modeled using a layered velocity structure in the source region, representing the Himalayan orogenic prism, the Indian upper and lower crust, and the Indian mantle, respectively [*Pandey et al.*, 1999; *Monsalve et al.*, 2008; *Nábělek et al.*, 2009] (Table S1). We constrain the absolute focal depths of moderate aftershocks (M_w5.5 to M_w6.3, Table S2) by modeling the teleseismic waveforms of the direct *P* and the surface reflections *pP* and *sP* (Figure 3) following *Kikuchi and Kanamori* [1991]. Using the depths determined by HYPOSAT and by waveform modeling, we calculate hypocenters of all earthquakes using a multiscale double-difference earthquake relocation method (Multi-DD) [*Bai and Zhang*, 2015], which is modified from the hypoDD programs [*Waldhauser*, 2001] to include phases recorded by regional and teleseismic networks. Since differential traveltimes do not depend strongly on the assumed velocity models along the whole raypath [*Waldhauser and Ellsworth*, 2000; *Waldhauser and Schaff*, 2007], the joint analysis of local, regional, and teleseismic data and the precise measurements of differential phase arrival times via waveform cross correction for the China-Nepal array (Figure S1) improve the relative focal depth determinations considerably. The focal depths for earthquakes determined by waveform modeling are held fixed during the Multi-DD processing to constrain the absolute focal depths of all earthquakes. We calculate differential traveltimes between each event and up to eight of its nearest neighbors. Each event pair has 8–32 commonly observed phases within a 15 km distance between the two events. The data include 9690 *Pg* and *Sg*, 5288 *Pn* and *Sn*, 174 *pP* and *sP*, and 17,664 teleseismic *P* and *S* arrival times.

4. Results

We estimate the uncertainty of the relocations by a bootstrap analysis [*Bai et al.*, 2006] using 100 sampling iterations (Figure S2). This analysis indicates that epicenters are estimated with an accuracy of ±3.5 km, which is 2 times smaller than the average uncertainty of ±7.0 km reported in the NEIC catalog. The uncertainty in the focal depth estimate is ±2.0 km, in agreement with the estimates of focal depth uncertainty based on waveform fits (Figure 3). The differential time residuals are reduced substantially from ±5 s before to ±1.5 s after relocations (Figure S3). The weighted L1 and L2 norm residuals decreased from 1.10 s and 1.58 s to 0.46 s and 0.60 s after relocations, respectively, demonstrating that the earthquakes are better relocated.

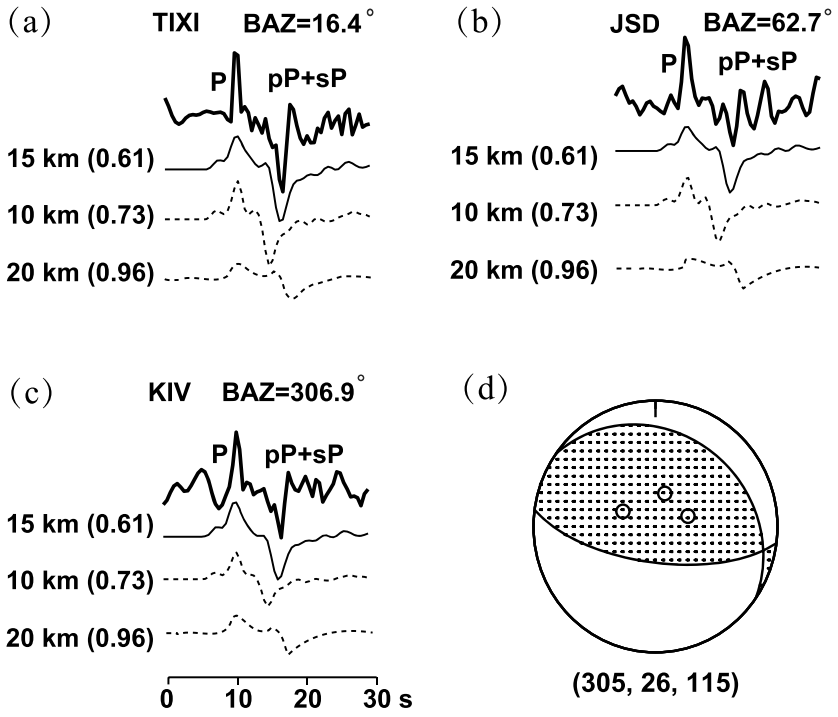

Figure 3. Comparison of the recorded (thick lines) and computed *P* waveform for event 98 (Table S2) at stations (a) TIXI, (b) JSD, and (c) KIV. Waveforms are band-pass filtered from 0.01 to 1 HZ. The preferred focal depth for this event is 15.5 km below the surface (thin lines) or 14.2 km beneath sea level. Waveform misfits for $H = 10$ km (0.73) and $H = 20$ km (0.96) are much higher because *pP* and *sP* phases in the data and the computed seismograms are misaligned. (d) Focal mechanism of the earthquake. Locations of the three stations shown in Figures 3a–3c are shown by open circles.

The average focal depth after relocation is 14.7 km below the surface, deeper than the default value of 10 km in the NEIC catalog for most of the aftershocks. Almost all aftershocks occurred to the southeast of the main shock. Few aftershocks occurred northeast of Kathmandu, where coseismic slip is large [*Avouac et al.*, 2015; *Fan and Shearer*, 2015; *Lindsey et al.*, 2015; *Wang et al.*, 2015; *Wang and Fialko*, 2015]. The M_w7.3 Kodari earthquake occurred on the eastern edge of the aftershock zone. We estimate the focal depth of the main shock to be 18.5 ± 2 km (Figure 3), consistent with the depth of the MHT [*Nábělek et al.*, 2009] and the locking line at the source region [*Bilham et al.*, 2001; *Avouac et al.*, 2015]. The focal depths of the M_w7.3 and M_w6.7 aftershocks

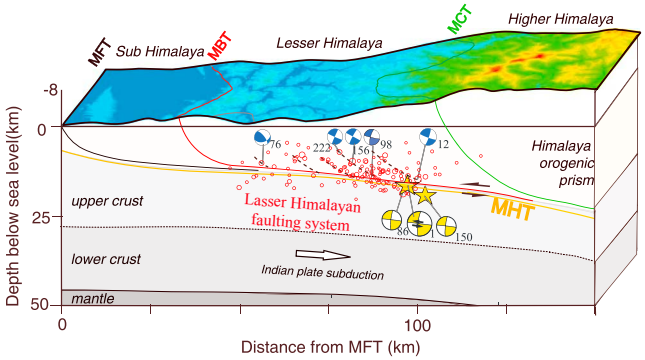

Figure 4. Cross section along the double lines in Figure 1 showing relocated earthquakes that occurred before the M_w 7.3 event. Yellow and blue earthquake focal mechanisms show events in cross-sectional view with dip angles of about 10° and 25°, respectively (http://www.globalcmt.org/). Numbers are the earthquake ID (Table S2 in the supporting information). The dotted black lines indicate the steeply dipping faults where aftershocks occurred within the Lesser Himalayan thrust system.

(events 150 and 86 in Table S2) are 21 km, slightly deeper than the depth of MHT near a patch of large slip below the plate surface [*Galetzka et al.*, 2015].

Figure 4 shows relocated hypocenters of the main shock and major aftershocks along a N20°E cross section perpendicular to the strike of the Gorkha main shock fault plane. Most aftershocks are shallower than the main shock and located in the hanging wall. They line up as clear north dipping structures with dip angles of about 25°, which is 15° steeper than the dip of the MHT [*Nábělek et al.*, 2009] and the shallow nodal plane of the main shock [*Avouac et al.*, 2015]. The steeper dips are in good agreement with the focal mechanism solutions of aftershocks 12, 76, 98, 156, and 222 (Table S2) reported in the global centroid moment tensor (gCMT) catalog.

5. Discussion and Conclusions

The 2015 Gorkha earthquake sequence on a shallow section of the MHT has been recorded extremely well by local, regional, and global seismic arrays. From precise relocations, we infer that the Gorkha aftershocks (Figure 1) are distributed above the anticlinorium system of the MCT. The southern edge of the aftershock zone is very close to the MBT [*Amatya et al.*, 1994], which is the thrust placing the lesser Himalaya over Tertiary sedimentary strata. *Pandey et al.* [1999] suggested that earthquakes along Himalaya orogeny are mostly parallel to the MBT. These observations indicate that the MBT may control earthquake occurrence along the frontal edge of the Himalaya.

While the main shock ruptured a section of the MHT, most of the aftershocks with M_w3.5 or larger have shallower focal depths and the northward dipping nodal planes of the largest aftershocks have larger dip angles. We infer therefore that the aftershocks are mainly distributed on steeper dipping structures within the hanging wall of the Lesser Himalaya (Figure 4).

Northward motion on the Indian plate was associated with the development of a thrust system that consists of both the near-horizontal MHT and more steeply dipping faults above. *Pandey et al.* [1999] and *Yin* [2006] suggested such a Lesser Himalayan duplex system to exist in the western Himalaya and to cause folding of the MCT and STD at deeper depth. The Gorkha aftershock locations indicate that this thrust system is also present in central Nepal.

Active faults exist throughout the Kathmandu basin [*Nakata et al.*, 1990]. However, strike-slip earthquakes on these near-vertical faults have not been recorded in the past 50 years [*Bai et al.*, 2016]. Great earthquakes in the past 200 years include the 26 August 1833 M_w8.0 event [*Bilham*, 1995] and the 15 January 1934 M_w8.0 Bihar-Nepal event [*Sapkota et al.*, 2012] (Figure 1), which have been attributed to slip on the MHT. Many of the historical large earthquakes along the Himalaya orogeny were located beneath the Lesser Himalaya [*Rajendran et al.*, 2015]. We infer that the Lesser Himalaya thrust system is the most seismically active region along the Himalaya convergence and accommodates most of the elastic strain accumulation of the region.

Acknowledgments

This research is funded by the grants of National Nature Science Foundation of China (41274086 and 41490611) and the Chinese Academy of Sciences (CAS: L. Bai) to L.B., the grant of National Nature Science Foundation of China (41174069) to H.L., and the grant of National Science Foundation of the U.S. (EAR-1416695) to J.R. We used earthquake catalogs from the reviewed ISC bulletin, CEDC, and NEIC, and waveform data from the Data Management Center of IRIS and CNSN at the Institute of Geophysics, China Earthquake Administration [SEISDMC, doi:10.7914/SN/CB *Zheng et al.*, 2010], respectively. We are grateful to the China-Nepal array team for conducting the field work.

References

Acton, C. E., K. Priestley, and V. K. Gaur (2011), Crustal structure of the Darjeeling-Sikkim Himalaya and southern Tibet, *Geophy. J. Int.*, *184*(2), 829–852, doi:10.1111/j.1365-246X.2010.04868.x.

Amatya, K., B. Jnawali, and P. Shrestha (1994), Geological map of Nepal: Kathmandu, 1994: Scale: 1: 1 000 000, Dep. of Mines and Geol., Kathmandu, Nepal.

Avouac, J. P., L. Meng, S. Wei, T. Wang, and J. P. Ampuero (2015), Lower edge of locked Main Himalayan Thrust unzipped by the 2015 Gorkha earthquake, *Nature Geosci.*, *8*, 708–711, doi:10.1038/ngeo2518.

Bai, L., and T. Zhang (2015), Complex deformation pattern of the Pamir-Hindu Kush region inferred from multi-scale double-difference earthquake relocations, *Tectonophysics*, *638*, 177–184, doi:10.1016/j.tecto.2014.11.006.

Bai, L., Z. Wu, T. Zhang, and I. Kawasaki (2006), The effect of distribution of stations upon location error: Statistical tests based on the double-difference earthquake location algorithm and the bootstrap method, *Earth Planets Space*, *58*, e9–e12.

Bai, L., G. Li, N. G. Khan, J. Zhao, and L. Ding (2016), Focal depths and mechanisms of shallow earthquakes in the Himalayan-Tibetan region, *Gondwana Res.*, doi:10.1016/j.gr.2015.07.009.

Bilham, R. (1995), Location and magnitude of the 1833 Nepal earthquake and its relation to the rupture zones of contiguous great Himalayan earthquakes, *Curr. Sci.*, *69*, 101–128.

Bilham, R. (2015), Raising Kathmandu, *Nature Geosci.*, *8*, 582–584.

Bilham, R., V. Gaur, and P. Molnar (2001), Himalayan seismic hazard, *Science*, *293*, 1442–1444.

Bollinger, L., S. N. Sapkota, P. Tapponnier, Y. Klinger, M. Rizza, J. Van der Woerd, D. R. Tiwari, R. Pandey, A. Bitri, and S. Bes de Berc (2014), Estimating the return times of great Himalayan earthquakes in eastern Nepal: Evidence from the Patu and Bardibas strands of the Main Frontal Thrust, *J. Geophy. Res. Solid Earth*, *119*, 7123–7163, doi:10.1002/2014JB010970.

Caldwell, W. B., S. L. Klemperer, J. F. Lawrence, S. S. Rai, and Ashish (2013), Characterizing the Main Himalayan Thrust in the Garhwal Himalaya, India with receiver function CCP stacking, *Earth Planet. Sci. Lett.*, *367*, 15–27.

Fan, W., and P. M. Shearer (2015), Detailed rupture imaging of the 25 April 2015 Nepal earthquake using teleseismic P waves, *Geophys. Res. Lett.*, *42*, 5744–5752, doi:10.1002/2015GL064587.

Galetzka, J., et al. (2015), Slip pulse and resonance of the Kathmandu basin during the 2015 Gorkha earthquake, Nepal, *Science*, *349*, 1091–1095.
Hand, E., and P. Pulla (2015), Nepal disaster predages a coming megaquake, *Science*, *348*, 484–485.
Hetényi, G., R. Cattin, F. Brunet, L. Bollinger, J. Vergne, J. L. Nábělek, and M. Diament (2007), Density distribution of the India plate beneath the Tibetan plateau: Geophysical and petrological constraints on the kinetics of lower-crustal eclogitization, *Earth Planet. Sci. Lett.*, *264*(1), 226–244.
Kikuchi, M., and H. Kanamori (1991), Inversion of complex body waves-III, *Bull. Seismol. Soc. Am.*, *81*(6), 2335–2350.
Kumar, S., S. G. Wesnousky, R. Jayangondaperumal, T. Nakata, Y. Kumahara, and V. Singh (2010), Paleoseismological evidence of surface faulting along the northeastern Himalayan front, India: Timing, size, and spatial extent of great earthquakes, *J. Geophy. Res.*, *115*, B12422, doi:10.1029/2009JB006789.
Lindsey, E. O., R. Natsuaki, X. Xu, M. Shimada, M. Hashimoto, D. Melgar, and D. T. Sandwell (2015), Line of sight displacement from ALOS-2 interferometry: M_w 7.8 Gorkha earthquake and M_w 7.3 aftershock, *Geophys. Res. Lett.*, *42*, 6655–6661, doi:10.1002/2015GL065385.
Monsalve, G., A. Sheehan, C. Rowe, and S. Rajaure (2008), Seismic structure of the crust and the upper mantle beneath the Himalayas: Evidence for eclogitization of lower crustal rocks in the Indian Plate, *J. Geophy. Res.*, *113*, B08315, doi:10.1029/2007JB005424.
Nábělek, J., G. Hetenyi, J. Vergne, S. Sapkota, B. Kafle, M. Jiang, H. Su, J. Chen, B. Huang, and H.-C. Team (2009), Underplating in the Himalaya-Tibet collision zone revealed by the Hi-CLIMB experiment, *Science*, *325*, 1371–1374.
Nakata, T., T. K. Otsuki, and S. H. Khan (1990), Active faults, stress field, and plate moltion along the Indo-Eurasian plate boundary, *Tectonophysics*, *181*, 83–95.
Ni, J., and M. Barazangi (1984), Seismotectonics of the Himalayan collision zone: Geometry of the underthrusting Indian plate beneath the Himalaya, *J. Geophy. Res.*, *89*(B2), 1147–1163.
Pandey, M. R., R. P. Tandukar, J. P. Avouac, J. Vergne, and T. Héritier (1999), Seismotectonics of the Nepal Himalaya from a local seismic network, *J. Asian Earth Sci.*, *17*(5), 703–712.
Rai, S. S., K. Priestley, V. K. Gaur, S. Mitra, M. P. Singh, and M. Searle (2006), Configuration of the Indian Moho beneath the NW Himalaya and Ladakh, *Geophy. Res. Lett.*, *33*, L15308, doi:10.1029/2006GL026076.
Rajendran, C. P., B. John, and K. Rajendran (2015), Medieval pulse of great earthquakes in the central Himalaya: Viewing past activities on the frontal thrust, *J. Geophys. Res. Solid Earth*, *120*, 1623–1641, doi:10.1002/2014JB011015.
Sapkota, S. N., L. Bollinger, Y. Klinger, P. Tapponnier, Y. Gaudemer, and D. Tiwari (2012), Primary surface ruptures of the great Himalayan earthquakes in 1934 and 1255, *Nat. Geosci.*, *6*, 71–76, doi:10.1038/NGEO1669.
Schelling, D., and K. Arita (1991), Thrust tectonics, crustal shortening, and the structure of the far-eastern Nepal, Himalaya, *Tectonicsics*, *10*, 851–862.
Schulte-Pelkum, V., G. Monsalve, A. Sheehan, M. R. Pandey, S. Sapkota, R. Bilham, and F. Wu (2005), Imaging the Indian subcontinent beneath the Himalaya, *Nature*, *435*, 1222–1225, doi:10.1038/nature03678.
Schweitzer, J. (2001), HYPOSAT-An enhanced routine to locate seismic events, *Pure Appl. Geophys.*, *158*, 277–289.
Waldhauser, F. (2001), hypoDD — A program to compute double-difference hypocenter locations (hypodd version 1.0-03/2001), *Open File Rep. USGS/OFR-01-113*, vol. 113, US Geol. Surv., Menlo Park, Calif.
Waldhauser, F., and W. L. Ellsworth (2000), A double-difference earthquake location algorithm: Method and application to the northern Hayward fault, California, *Bull. Seismol. Soc. Am.*, *90*(6), 1353–1368.
Waldhauser, F., and D. Schaff (2007), Regional and teleseismic double-difference earthquake relocation using waveform cross-correlation and global bulletin data, *J. Geophy. Res.*, *112*, B12301, doi:10.1029/2007JB004938.
Wang, K., and Y. Fialko (2015), Slip model of the 2015 M_w7.8 Gorkha (Nepal) earthquake from inversions of ALOS-2 and GPS data, *Geophys. Res. Lett.*, *42*, 7452–7458, doi:10.1002/2015GL065201.
Wang, W., J. Hao, J. He, and Z. Yao (2015), Rupture process of the M_w7.9 Nepal earthquake April 25, 2015, *Sci. China Earth Sci.*, *58*, 1895–1900, doi:10.1007/s11430-015-5170-y.
Xu, Q., J. Zhao, X. Yuan, H. Liu, and S. Pei (2015), Mapping crustal structure beneath southern Tibet: Seismic evidence for continental crustal underthrusting, *Gondwana Res.*, *27*, 1487–1493.
Yin, A. (2006), Cenozoic tectonic evolution of the Himalayan orogen as constrained by along-strike variation of structural geometry, exhumation history, and foreland sedimentation, *Earth Sci. Rev.*, *76*(1), 1–131.
Zhao, W., K. D. Nelson, and Project INDEPTH Team (1993), Deep seismic reflection evidence for continental underthrusting beneath southern Tibet, *Nature*, *366*, 557–559.
Zheng, X., Z. Yao, J. Liang, and J. Zheng (2010), The role played and opportunities provided by IGP DMC of China National Seismic Network in Wenchuan earthquake disaster relief and researches, *Bull. Seismol. Soc. Am.*, *100*, 2866–2872, doi:10.1785/012009025.